Stress Distribution and the Fragility of Supercooled Melts

Dmytro Bevzenko and Vassiliy Lubchenko*

Department of Chemistry, University of Houston, Houston, Texas 77204-5003

Received: July 24, 2009; Revised Manuscript Received: October 11, 2009

We formulate a minimal ansatz for local stress distribution in a solid that includes the possibility of strongly anharmonic short-length motions. We discover a broken-symmetry metastable phase that exhibits an aperiodic, frozen-in stress distribution. This aperiodic metastable phase is characterized by many distinct, nearly degenerate configurations. The activated transitions between the configurations are mapped onto the dynamics of a long-range classical Heisenberg model with 6-component spins and anisotropic couplings. We argue the metastable phase corresponds to a deeply supercooled nonpolymeric, nonmetallic liquid and further establish an order parameter for the glass-to-crystal transition. The spin model itself exhibits a continuous range of behaviors between two limits corresponding to frozen-in shear and uniform compression/dilation, respectively. The two regimes are separated by a continuous transition controlled by the anisotropy in the spin−spin interaction, which is directly related to the Poisson ratio σ of the material. The latter ratio and the ultraviolet cutoff of the theory determine the liquid configurational entropy. Our results suggest that liquid's fragility depends on the Poisson ratio in a nonmonotonic way. The present ansatz provides a microscopic framework for computing the configurational entropy and relaxational spectrum of specific substances.

If cooled sufficiently rapidly, a liquid may fail to crystallize but will instead remain in a metastable, *supercooled* state. Upon further cooling, the relaxation times in a supercooled liquid grow very rapidly as the mass transport becomes activated, in contrast with the mainly collisional transport near the fusion temperature. Because the local structures are much longer-lived than the vibrational equilibration times, the activated-transport regime represents a state with a broken translational symmetry, even though the corresponding, aperiodic structure shows no obvious distinction from a snapshot of an ordinary, uniform liquid. (It is said the heterogeneity is "dynamical".) Since the symmetry is broken *gradually* with lowering temperature, beginning with the highest frequency motions, a transition into this "aperiodic-crystal" state is not sharp but, instead, is a soft crossover centered at a temperature T_{cr},[1,2] corresponding universally to viscosity 10 Ps or so.[2,3] The crossover into the activated regime is a finite-dimensional analog of a mean-field kinetic catastrophe of the mode-coupling theory (MCT), whereby the motional barriers would diverge at a temperature T_A, even though the configurational entropy is still extensive.[4,5]

In additional contrast to the mean-field transition at T_A, the crossover at T_{cr} exhibits two emerging length scales: One length scale is the molecular length a that signifies the volumetric size of a chemically rigid unit, often called the "bead", that is not significantly perturbed during activated transport. Conversely, the beads interact with each other weakly, comparably to the Lennard-Jones interaction.[2] The bead may be thought of as a coarse-graining length, beyond which activated motions are largely independent of chemical detail, but fully characterized by a single, *bulk* quantity. This bulk quantity is the excess liquid entropy relative to the corresponding crystal, usually called the configurational entropy. The magnitude of the configurational entropy per bead, s_c, directly gives the number of alternative aperiodic configurations available to a region of a supercooled liquid containing N beads, i.e., $e^{s_c N/k_B}$. The bead usually contains two to three atoms but could be bigger for molecular liquids containing large rigid units such as benzene. The other length scale emerging during the crossover is the so-called Lindemann length d_L,[1,6,7] which is the molecular displacement at the mechanical stability edge. This length is nearly universal, $d_L \simeq a/10$, and characterizes bead displacements during transitions between distinct aperiodic packings in the metastable, aperiodic crystal phase. One may view the crossover into the activated liquid regime as a "localization" transition, whereby the emerging metastability of local structures is signaled by a *discontinuous* transition from a uniform liquid to a state with a nonzero force constant of the Einstein oscillator.[1] The random first-order transition (RFOT) theory utilizes this view to analyze the activated transport in chemically distinct (nonpolymeric) fluids in a *unified* fashion.[8−10] (See ref 11 for a review.) The RFOT theory predicts that in a fully developed activated regime, the structural relaxation time is determined solely by the configurational entropy per bead:[2,9]

$$\tau = \tau_{vibr} \exp(32 k_B/s_c) \qquad (1)$$

where $\tau_{vibr} \simeq 1$ ps is the microscopic time scale characterizing vibrational relaxation. By eq 1, system-specific deviations from the pure Arrhenius temperature dependence of τ result from variations in the value of the heat capacity jump at the glass transition temperature T_g per bead: $\Delta c_p \equiv T(\partial s_c/\partial T)|_{T=T_g}$. The so-called fragility index $m \equiv \mathrm{d}(\log \tau)/T\mathrm{d}(1/T)|_{T=T_g}$ gives a quantitative measure of that deviation. Small and large deviations from the Arrhenius T-dependence (corresponding to small and large m, respectively) are often called strong and fragile behaviors.[12,13] The RFOT theory predicts $m \simeq 34.7\Delta c_p$,[2,9,14] in excellent agreement with experiment.

Hall and Wolynes have put forth a simple specific model that relates the degree of molecular connectivity to the heat capacity jump Δc_p.[15] Establishing such connections between local chemistry and thermodynamics for actual substances is difficult, however, hampering our efforts to make first principles estimates of the configurational entropy and, ultimately, the glass-forming

* Corresponding author.

10.1021/jp9070345
Published on Web 12/02/2009

ability of those substances. Indeed, since the viscosity is directly related to the average relaxation time,[16]

$$\eta = \frac{2k_BT}{\pi a d_L^{\,2}}\langle\tau\rangle \simeq 60\frac{k_BT}{a^3}\langle\tau\rangle \qquad (2)$$

the crystal nucleus growth, which is subject to viscous drag,[17] is determined by the configurational entropy s_c per bead. The actual chemical identification of beads is relatively straightforward in molecular, but less so in covalently bonded, compounds, where, for instance, the apparent bead often corresponds to a noninteger fraction of a stoichiometric unit.[2,18] We note that these challenges are, of course, not unique to theories of the glass transition but equally pertain to quantitative descriptions of the ordinary liquid-to-crystal transition. Yet perhaps in reflection of these open questions, which we view as quantitative, many believe fragile and strong behaviors actually have distinct mechanisms.

In an effort to develop a microscopic description of the configurational dynamics in specific substances, here we propose and work out several consequences of a novel quasi-continuum ansatz for local stress distribution that implements direct interactions in the activated regime semiempirically, via the local elastic properties of the material. The ansatz incorporates the possibility of local, short-length motions that are similar in spirit to Einstein oscillators but are strongly anharmonic and account explicitly for the tensorial nature of the relation between local deformation and stress in solids. In particular, explicitly treated is (high-frequency) *shear* resistance, which is characteristic of deeply supercooled liquids and, generally, activated liquid transport. This fully tensorial treatment of stress may be viewed, among other things, as a systematic improvement on self-consistent scalar-phonon theories of aperiodic crystals.[1,19]

The many-body effects that lead to the emergence of shear resistance in liquids at high densities do not lend themselves easily to perturbative treatments that use the uniform liquid as the reference state. In contrast, we use a fully mechanically stable state as the reference state, and then uniformly allow for local, short-length anharmonic motions. Within this ansatz, a *metastable*, aperiodic frozen-in stress pattern emerges self-consistently, whereby the bead size is identified as the typical length scale of the stress heterogeneity. This result implies that even in a covalently bonded material, the concept of a bead is entirely unambiguous. The frozen-in stress pattern is multiply *degenerate*, whereby the transitions between alternative configurations can be mapped onto the dynamics of a classical Heisenberg model with six-component spins. The six components correspond to the independent entries in the local frozen-in deformation tensor. The average length of the spin emerges as an order parameter for the aperiodic-to-periodic crystal transition. The transitions between different spin configurations are rare events, implying the corresponding liquid states are long-lived and thus supporting the view of liquids in the activated-transport regime as aperiodic crystals. In other words, we explicitly confirm the nontrivial notion of the RFOT theory that aperiodic molecular assemblies can exhibit multiple states and, at the same time, support shear.

Already in a mean-field analysis of the spin model, we establish that the broken-symmetry state can exhibit a range of behaviors interpolating between frozen-in shear and uniform compression/dilation. These two limits correspond to 5-component Heisenberg- and Ising-like ferromagnets, respectively. The resulting heat capacity variations, together with the RFOT-derived intrinsic relation between thermodynamics and kinetics, as reflected in the m vs Δc_p relation, implies that the spin model exhibits a broad range of fragile-to-strong behaviors during activated rearrangements. The heat-capacity jump per bead of the corresponding liquid will also depend on the ultraviolet cutoff of the theory, as specified by the bead size. We will observe that the fragility depends on the Poisson ratio of the material, but in a complicated, nonmonotonic fashion. In any case, in view of the apparent broad range of strong-to-fragile behaviors exhibited in the present model, the present analysis strongly suggests the activated dynamics have the same mechanism in both strong and fragile liquids, consistent with the basic picture of the RFOT theory.

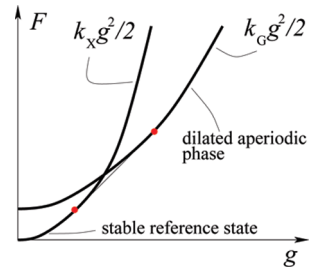

Figure 1. Illustration of the notion of an aperiodic metastable state as a dilated crystal that was allowed to relax.

A potential formal benefit of the present approach is that it is possible to map the activated-transport liquid regime onto a spin model on a *fixed* lattice, thus opening the possibility of applying to liquids the many computational techniques developed in the context of spin models. Importantly, this mapping may provide a first principles basis for computing the configurational entropy for specific substances and the rate of crystallization from the supercooled state, since elastic constants at the length scale of a bead, which are the input into the theory, can be determined by ab initio methods.

1. Microscopic Ansatz for Local Stress Distribution

Let us begin with an *informal motivation* for an ansatz for local stress distribution in a glass. Consider a substance that can both crystallize and vitrify and assume for concreteness that the glass has a greater specific volume than the corresponding crystal, as is usually the case. A quenched melt or frozen glass of such a substance may be thus viewed as a result of the following action: Apply negative pressure to slowly expand the crystal until the lattice relaxes into one of the myriad available glass structures, and then release the negative pressure. (We assume cracking does not occur.) The sample will remain in the metastable, glass state; the eventual transition to the lower free energy, crystal state will occur by nucleation and is subject to the surface tension between the two phases. In a standard fashion, the surface tension implies that the dependence of the free energy on the extent of dilation exhibits a nonconcave portion.[20] (By "concave", we will consistently mean concave-*up*.)

We can see qualitatively how the nonconcavity arises by estimating the free energy of the solid using a simple *nonlinear* Einstein-oscillator model. Suppose the configurational partition function of each oscillator is $\int_g^\infty \mathrm{d}^3\mathbf{r}\ \mathrm{e}^{-kr^2/2k_BT}$, where we incorporate the nonlinearity qualitatively by assuming a hard lower cutoff in the configurational integral, at a displacement g. k is the force constant in the harmonic limit. Denote the force constants in the crystal and the expanded state as k_X and k_G, respectively. Clearly, $k_G < k_X$. We sketch the free energies of the states as functions of g in Figure 1, taking into account that the curve corresponding to the expanded state is shifted upward

from the crystal state by the free energy cost of expansion. According to Figure 1, under sufficient negative pressure (essentially equal to the negative slope of the common tangent of the two curves), the crystal will indeed begin converting into a collection of nonlinear oscillators. The vast majority of the configurations of these oscillators are of course aperiodic, implying the metastable phase is aperiodic too. This qualitative free energy graph tentatively confirms the view above of a quenched-melt/frozen-glass as a sufficiently expanded crystal that was allowed to relax. The graph also suggests an appropriate order parameter for the transition, namely the amplitude of short-wavelength, strongly anharmonic motions.

In writing a *formal* ansatz for a solid that allows short length anharmonic motions, we first point out that local mechanical instabilities are perfectly compatible even with macroscopic rigidity, examples including orientational glasses[21] and ferroelectrics of order−disorder type.[22−24] The latter systems consist of rigid, periodic scaffolds where a *subset* of local motions could be marginally stable (resulting in a vanishing frequency of transverse optical phonons[22]) or even multistable. In contrast, we wish to consider here a situation where *all* short length motions are allowed to be multistable. The resulting material may or may not be macroscopically stable, as will be determined self-consistently. We will limit ourselves to a dynamical regime, in which relative distortions of individual bonds during lattice reconfigurations are only within 10% or so,[1,6,7] as appropriate for both activated transport and stable crystals. Such small distortions imply the harmonic approximation for local stress is semiquantitative. Take the Landau local free energy density as a function of the local deformation profile u_{ij}: $f = {}^1/_2 u_{ij}\Lambda_{ijkl}u_{kl}$, where Λ_{ijkl} is the standard elastic tensor and the Einstein's summation convention for *Latin* indeces is implied.[25] ($u_{ij} \equiv {}^1/_2(\partial u_i/\partial x_j + \partial u_j/\partial x_i)$, $i, j = 1, 2, 3$, where u is the local displacement relative to a steady-state reference state.)

Decompose the deformation tensor into long- and short-wavelength components: $u_{ij} = u_{ij}^{<} + d_{ij}$, where $u_{ij}^{<}$ only includes Fourier components with wave-vectors within a certain cutoff surface in k-space, while d_{ij} contains only Fourier components outside of the cutoff surface. Let us evaluate the free energy of the system subject to a constraint on the self-energy of the local motions $d_{ij}\Lambda_{ijkl}d_{kl} = g^2$, thus forcing the short-length motions to be essentially anharmonic Einstein oscillators. If the cutoff surface in the Fourier space is generically at $k \simeq k_{\text{micro}}$, the anharmonic oscillators fill the space, approximately one per volume $(\pi/k_{\text{micro}})^3$, but not necessarily in a periodic fashion. The detailed lattice in which the oscillators are arranged depends on the precise shape of the cutoff surface. Since the presence of strongly anharmonic degrees of freedom generally requires expanding the lattice from the reference state, owing to steric repulsion, we must include in the full free energy of our solid a penalty for increasing g, which we denote as $F_{\text{ex}}(g)$. The precise form of this function is not essential for the majority of our conclusions; clearly it is a monotonically increasing, *concave* function of g, to ensure the compressibility is positive. As a result, the full free energy is

$$F(g) = F_0(g) + F_{\text{ex}}(g) \tag{3}$$

where the free energy of the ansatz F_0 is computed by summing over all configurations of local stress at temperature $T \equiv 1/k_B\beta$:

$$e^{-\beta F_0(g)} = \sum_{\{\mathbf{u}(\mathbf{r}),\mathbf{d}(\mathbf{r})\}} e^{-\beta \int dV f(\mathbf{r})} \tag{4}$$

subject to the constraint

$$d_{ij}(\mathbf{r})\Lambda_{ijkl}d_{kl}(\mathbf{r}) = g^2(\mathbf{r}) \tag{5}$$

The local free energy density $f(\mathbf{r})$ of a particular stress configuration at site is

$$f(\mathbf{r}) = \frac{1}{2}(u_{ij} + d_{ij})\Lambda_{ijkl}(u_{kl} + d_{kl}) \tag{6}$$

We have dropped the superscript "<" from the long-wavelength, "acoustic" component of the total deformation $u^{<}$, to simplify notation. For the sake of argument, we will assume the order parameter is uniform:

$$g^2(\mathbf{r}) = g^2 \tag{7}$$

Formal extension to a nonuniform $g(\mathbf{r})$ is straightforward.

In the following, it will be often convenient to present the six independent entries of the symmetric tensors u_{ij} and d_{ij} as 6-component vectors, which is sometimes referred to as the Voigt (or Voigt−Mandel) notation.[26,27] Here we choose the specific realization of the Voigt notation, in which the tensor Λ is a second rank (positively defined) *tensor* of size 6×6. Upon a suitable linear transformation (see Appendix A), we can formally rewrite eq 6 as

$$f(\mathbf{r}) \equiv f_{\vec{\phi},\vec{g}}(\mathbf{r}) = \frac{1}{2}(\vec{\phi} + \vec{g})^2 \tag{8}$$

where

$$\phi^2 \equiv \sum_{\alpha=1}^{6} \phi_\alpha{}^2 = u_{ij}\Lambda_{ijkl}u_{kl} \tag{9}$$

and

$$g^2 \equiv \sum_{\alpha=1}^{6} g_\alpha{}^2 = d_{ij}\Lambda_{ijkl}d_{kl} \tag{10}$$

Throughout the article, we will consistently indicate 6-component vectors with arrows, $\vec{g} = \Sigma_{\alpha=1}^{6} g_\alpha \vec{e}_\alpha$, where $\vec{e}_\alpha\vec{e}_\beta = \delta_{\alpha\beta}$, and three component vectors with bold symbols, $\mathbf{u} = u_i\mathbf{e}_i$, where $\mathbf{e}_i\mathbf{e}_j = \delta_{ij}$. We will not apply the Einstein summation convention to Greek indeces.

Even though we have written $\vec{g}(\mathbf{r})$ (or $d_{ij}(\mathbf{r})$) as a continuum field, it is understood that $\vec{g}(\mathbf{r})$ actually stands for a discrete vector located at the site of the lattice of the nonlinear Einstein oscillators that is closest to the point $\mathbf{r}$ in space. Switching between discrete summation over lattice sites and continuous integration over space is straightforward: If the volume occupied by a single vector $\vec{g}$ is a^3, implying $k_{\text{micro}} \simeq \pi/a$, we may interchange the summation and integration according to $a^3\Sigma \leftrightarrow \int dV$. Since vectors $\vec{g}$ correspond to 6 degrees of freedom, the region corresponding to one vector $\vec{g}$ must contain at least *two* atoms. $\vec{\phi}(\mathbf{r})$ (or $u_{ij}(\mathbf{r})$) is of course, too, an approximation to acoustic modes of a *discrete* lattice, at wavelengths exceeding $2\pi/k_{\text{micro}}$. Note that the number of these acoustic modes is three per vector $\vec{g}(\boldsymbol{r})$, corresponding to the three translational degrees of freedom of the vector-containing region.

For the sake of argument we will consider the simplest case of an isotropic reference state:

$$\Lambda_{ijkl} = \lambda\delta_{ij}\delta_{kl} + \mu(\delta_{ik}\delta_{jl} + \delta_{il}\delta_{jk}) \tag{11}$$

where λ and μ are the Lamé coefficients.[25] μ is also called the shear modulus. In the isotropic case, the components of vectors $\vec{\phi}$ and $\vec{g}$ have a particularly lucid meaning. One component, called "dilatational", corresponds to uniform compression:

$$g_1^2 = Kd_{ii}^2 \tag{12}$$

and the rest five, called "isochoric", to pure shear:

$$\sum_{\alpha=2}^{6} g_\alpha^2 = 2\mu\left(d_{ij} - \frac{1}{3}\delta_{ij}d_{ll}\right)^2 \tag{13}$$

where $K \equiv [\lambda + (2/3)\mu]$ is the usual bulk modulus.[25]

2. Glass as a Frozen-In, Multiply Degenerate Stress Pattern

We inquire about the possibility of (metastable) states with nonzero g by testing for nonconcavity of $F(g)$ from eq 3. The latter peculiarity is only possible if $F_0(g)$ has an inflection point. An analytic evaluation of $F_0(g)$ appears difficult (except in the mean-field limit, see next section). Despite the simple bilinear form in eq 6, the functional integration over $\mathbf{u}(\mathbf{r})$ in eq 5 at a fixed configuration $d_{ij}(\mathbf{r})$ could not be performed by simply changing variables $\mathbf{u} = \mathbf{u}' - \mathbf{d}$ and performing a Gaussian integration with respect to the new variable $\mathbf{u}'$: In contrast to the purely harmonic, long-wavelength motions $\mathbf{u}$, the new displacement field $\mathbf{u}'$ would now contain short-wavelength motions, which, by construction, are anharmonic.

It will suffice for our purposes here to extract the small and large g asymptotics of $F_0(g)$, which one may accomplish by first averaging the Boltzmann weight $e^{-\beta\int dV f(\mathbf{r})}$ from eq 4 over the *directions* of the $\vec{g}$ vectors on each site. By the aforementioned prescription for interchange between discrete summation over the oscillator sites and integration in space, we break up the integral in the exponent into a sum $\Sigma_i a^3 f(\mathbf{r}_i)$. Note the formula $\langle \exp(\vec{x}\vec{y})\rangle = I_{m/2-1}(xy)(xy/2)^{1-m/2}\Gamma(m/2)$, where the averaging $\langle\cdots\rangle$ is with respect to the mutual angle between two m-component vectors $\vec{x}$ and $\vec{y}$ (see ref 28 or formula 9.6.18 of ref 29). Here, $I_\nu(x)$ is the modified Bessel function of the first kind of order ν and Γ is the gamma function.[29] Using this formula, we average $e^{-\beta a^3\vec{\phi}\vec{g}}$ over the directions of $\vec{g}$ on each site and obtain the following free energy at site, per nonlinear oscillator:

$$f_{\phi,g}(\mathbf{r}) = \frac{1}{2}[\phi^2(\boldsymbol{r}) + g^2] - \frac{1}{\beta a^3}\ln\frac{I_2[\beta a^3\phi(\mathbf{r})g]}{[\beta a^3\phi(\mathbf{r})g]^2} \tag{14}$$

up to an additive constant. The subscripts ϕ, g at $f_{\phi,g}(\mathbf{r})$ above signify that the latter function is derived from the original free energy density $f(\mathbf{r})$ from eq 8 but now depends only on the absolute values of the 6-component vectors $\vec{\phi}$ and $\vec{g}$ characterizing the long- and short-wavelength distortions respectively. We note that expression 14 represents the exact free energy of our ansatz, up to the small numerical ambiguities related to the detailed shape of the cutoff surface in the Fourier space and the lattice of the spins.

To extract the small g behavior of $F_0(g)$, we note that at small values of either field, expression 14 yields

$$f_{\phi,g}(\mathbf{r}) \xrightarrow{\phi g\to 0} \frac{1}{2}\phi^2(\mathbf{r})\left(1 - \frac{g^2\beta a^3}{6}\right) + \frac{1}{2}g^2 \tag{15}$$

implying that the sole effect of the presence of the (small) short-wavelength anharmonic displacement of magnitude g is a renormalization of all acoustic frequencies downward by a factor of $(1 - g^2\beta a^3/6)^{1/2} \simeq (1 - g^2\beta a^3/12)$. Since the partition function of a classical harmonic oscillator with frequency ω is $(k_BT/\hbar\omega)$, this reduction in the acoustic frequency results in a free energy shift of $-k_BT(g^2\beta a^3/12)$ per phonon. As mentioned earlier, the number of the acoustic modes is 3 times the number of vectors $\vec{g}$, yielding that at small g, $f(g) \simeq g^2/2 - 3(k_BT/a^3)(g^2\beta a^3/12) = g^2/4$. Thus at small g, the second derivative of $F_0(g)$ is positive.

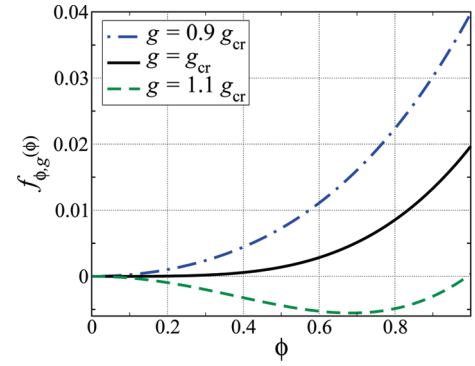

Figure 2. Free energy profiles for local elastic strain at three representative values of the anharmonic displacement g, from eq 14. Above the critical value g_{cr} from eq 17, the lattice freezes in an aperiodic pattern at wavelength $2\pi/k_{micro}$.

According to the asymptotic expansion of the Bessel function, $I_\nu(x) \propto e^x/x^{1/2}$,[29] the two leading terms in the large g limit of eq 14 are given by

$$f_{\phi,g}(\mathbf{r}) \xrightarrow{g\to\infty} \frac{1}{2}[|\vec{\phi}(\mathbf{r})| - g]^2 + \frac{5}{2}\frac{k_BT}{a^3}\ln g \tag{16}$$

In contrast with eq 6), the g-dependent portion of the free energy is now uniform in space and thus no longer has short-wavelength components. As a result, we can always shift the u variable to eliminate the g dependence from the integrand in the partition function corresponding to the free energy (16) so as to make the expression a pure quadratic in the new variable ϕ': $\mathbf{u} = \mathbf{u}_0 + \mathbf{u}' \Rightarrow \vec{\phi} = \vec{\phi}_0 + \vec{\phi}'$ where $|\vec{\phi}_0| = g$. (This latter reference state physically corresponds to a uniform distribution of stress (not displacement!) at free energy density $g^2/2$.) The resulting integration is ϕ' becomes asymptotically Gaussian in the large g limit, despite the nonanalytical dependence on $\vec{u}$ in eq 16). As a result, $f_g(g) \xrightarrow{g\to\infty} (5/2)(k_BT/a^3)\ln g$; i.e., the second derivative of $F_0(g)$ becomes negative at large g, implying $F_0(g)$ has an inflection point at an intermediate value of g.

We thus conclude from the analysis of the asymptotic behavior of the free energy $F_0(g)$ that with a suitable form of $F_{ex}(g)$, such as $F_{ex}(g) \propto g^2$, it is possible for the full free energy $F(g)$ to have a nonconcave portion, also consistent with the mean-field solution in section 3; see Figure 5. We reiterate that the presence of the nonconcave portion means the system exhibits a metastable state at a *nonzero* value of g. The latter quantity therefore can be used as an order parameter for a transition between the lowest free energy, fully stable state and the metastable state at nonzero g.

The free energy of our ansatz, eq 14, helps us understand the origin of the peculiar behavior of $F_0(g)$. Indeed, at large enough magnitude of anharmonic displacement, g, the equilibrium value of the acoustic displacements becomes nonzero. According to eq 15 this transition occurs at a critical value:

$$g_{cr}^2 = \frac{6k_BT}{a^3} \tag{17}$$

We show the ϕ dependence of the free energy from eq 14 in Figure 2, for several representative values of g. Note that the critical value of the excess free energy at a single vector, $a^3 g_{cr}^2/2 = 3k_BT$, is the total energy of a single atom in a harmonic lattice.

In the metastable phase at $g > 0$, the thermodynamic potential from eq 14 is dominated by aperiodic configurations of $\vec{g}$'s, implying the modulation of the harmonic field is aperiodic, too. This potential becomes particularly vivid in the $g^2/k_BT \rightarrow \infty$ limit, i.e., $(g - |\vec{\phi}|)^2/2 \equiv [g - (u_{ij}\Lambda_{ijkl}u_{kl})^{1/2}]^2/2$. This form means that the aperiodic phase corresponds to a frozen-in stress pattern at half-wavelength $a = \pi/k_{\text{micro}}$, which we must thus associate with the bead size of the RFOT theory. Consistent with this identification, the form $[g - (u_{ij}\Lambda_{ijkl}u_{kl})^{1/2}]^2$ is similar to broken-symmetry functionals that arise in systems with self-generated disorder.[30,31] Importantly, the free energy (14) is an equilibrium quantity, implying the metastable aperiodic state corresponds to a melt *above* the glass transition.

The aperiodic phase exhibits many distinct states separated by activation barriers. To see this structural degeneracy explicitly, we first integrate out the acoustic deformation in eq 4 at a fixed $d_{ij}(\mathbf{r})$ configuration. Analogous calculations have been performed, for instance, by Grannan at el.,[32,33] who have considered defect-phonon couplings in the form of $Q_{ij}u_{ij}$. Using their result or by straightforward path-integration in k-space (see Appendix B), we obtain the following effective Hamiltonian that couples the nonlinear oscillators, in the tensorial and Voigt notations respectively:

$$\begin{aligned} \mathscr{H}_{\text{spin}} &= -\sum_{m<n} a^3 K_{ijkl}(\mathbf{r}_m - \mathbf{r}_n) d_{ij}^{(m)} d_{kl}^{(n)} \\ &\equiv -\sum_{m<n} \sum_{\alpha,\beta=1}^{6} a^3 J_{\alpha\beta}(\mathbf{r}_m - \mathbf{r}_n) g_\alpha^{(m)} g_\beta^{(n)} \end{aligned} \tag{18}$$

where the double $(m < n)$ sums are over all bead pairs and the spin−spin coupling is the Fourier transform:

$$K_{ijkl}(r) \equiv \int_0^{k_{\text{micro}}} \frac{d^3(\mathbf{k}a)}{(2\pi)^3} \cos(\mathbf{kr}) \tilde{K}_{ijkl} \tag{19}$$

of the following tensor:

$$\tilde{K}_{ijkl} = \frac{\hat{k}_p \hat{k}_q}{\mu} \left(\Lambda_{ijmp}\Lambda_{klmq} - \frac{\lambda + \mu}{\lambda + 2\mu} \Lambda_{ijmp}\Lambda_{klnq}\hat{k}_m\hat{k}_n \right) \tag{20}$$

where $\hat{\mathbf{k}} \equiv \mathbf{k}/k$ and the tensor Λ_{ijkl} is from eq 11. The Fourier image $\tilde{J}_{\alpha\beta}(\mathbf{k})$ of the interaction $J_{\alpha\beta}(\mathbf{r})$ from eq 18 is a dimensionless 6×6 matrix, which means here that the interaction between the spins scales as $1/r^3$ at large distance, similarly to the usual dipole−dipole interaction.

We note that Hamiltonians similar to that in eq 18 have been employed in the context of configurational glasses.[32,34] Those treatments were restricted to defects of the type $Q_{ij} \propto [n_i n_j - (1/3)\delta_{ij}]$, where $\mathbf{n}$ is a *three*-component unit vector corresponding to the orientation of a polar group. Grannan at el.[32] point out that magnets of the type in eq 18 are frustrated even on periodic lattices.

The classical Heisenberg-like ferromagnet from eq 18 exhibits many distinct states separated by barriers, below its Curie temperature. (See next section for the mean-field phase-diagram of the model.) These distinct states correspond to distinct configurations in the corresponding quenched liquid. The bead motions during transitions between these distinct states correspond to rotations of the six-component, classical "spins" $\vec{g}^{(m)}$. The relative displacement of two beads, e.g., m and n, during a transition is related to the transition-induced change in the vector $(\vec{g}^{(m)} - \vec{g}^{(n)})$. The relation, however, is not obvious because of the tensorial nature of the frozen-in stress resulting in vectors being six-component. As in any magnet below its ordering transition, *typical* transitions between distinct metastable states of the spin system from eq 18 will involve the more spins the lower the temperature. Such bigger cooperative regions are necessary because the density of states for a region of fixed size decreases dramatically for lower energies. Specifically, according to the RFOT theory, the cooperativity size in the present case should increase as $1/s_c^{2/3}$,[8] where s_c is the entropy per bead (spin). Consistent with the cooperativity, the individual vectors rotate little relatively to each other so as to minimize local strain, implying the beads will move nearly harmonically most of the time. The transition is, nevertheless, strongly anharmonic, as reflected in a high free energy barrier for the reconfiguration. An appropriate progress coordinate is the number of beads that have already moved.[10]

We conclude this section by pointing out that the obtained mapping between activated liquid transport and the dynamics of the 6-spin Hamiltonian from eq 18 is not exact, of course, but nonetheless does capture the essential features of the activated-transport regime in liquids. Systematic improvements, such as using a more flexible functional form for the nonlinear oscillators, including higher order multipole terms in the spin−spin interaction, etc., are possible; however, they will result in largely quantitative corrections.

3. Mean-Field Analysis of the Spin Model

It is straightforward to show that the Fourier image $\tilde{J}_{\alpha\beta}(\mathbf{k})$ of the interaction $J_{\alpha\beta}(\mathbf{r})$ from eq 18 has the simple property $\tilde{J}^2 = \tilde{J}$ (i.e., $\Sigma_\beta \tilde{J}_{\alpha\beta}\tilde{J}_{\beta\gamma} = \tilde{J}_{\alpha\gamma}$) and that the trace of the $\tilde{J}$ matrix equals three for any value of the wave-vector $\mathbf{k}$. These two notions imply the matrix $\tilde{J}$ has two eigenvalues: 1 and 0, both triply degenerate. For comparison, the analogous matrix for the regular *elastic* dipole−dipole interaction between 3-component spins, $\hat{k}_i\hat{k}_j$ (see Appendix B), has eigenvalues 1, 0, 0. For the *electric* dipole−dipole interaction, the eigenvalues are −1, 0, 0. We thus conclude that in the sense that electric dipoles form an *anti*-ferromagnet (for not too oblong samples)[35] the Hamiltonian from eq 18 corresponds to a ferromagnet. (This difference can be understood as stemming from the notion that in phonon-mediated interactions, it is *like*-charges that attract, in contrast with the Coulomb law.)

In a mean-field limit, when the interaction $J_{\alpha\beta}(\mathbf{r})$ from eq 18 does not depend on the mutual separation $\mathbf{r}$ between spins, the Hamiltonian (18) indeed becomes a simple ferromagnet. This limit may be formally implemented by taking the $k_{\text{micro}} \rightarrow 0$ limit in eq 19 while renormalizing the integrand so that the total energy of the system is finite and scales with the total number of the 6-spins. Under these circumstances, the k-integration in eq 20 reduces to angular averaging of the $\tilde{K}$ tensor. Upon the averaging, as outlined in Appendix B, the $\tilde{J}$ tensor becomes a diagonal matrix with eigenvalues that turn out to be dimensionless combinations of the microscopic elastic constants: one eigenvalue corresponding to uniform compression: $K/(\lambda + 2\mu)$, and a 5-fold degenerate eigenvalue corresponding to pure shear: $(2/5)(K + 2\mu)/(\lambda + 2\mu)$. In other words, in the mean field limit, the dilatational components of local stress on one site do not interact with the isochoric components of local stress on another site.

As a result, the mean-field limit of the Hamiltonian (18) is

$$\mathscr{H}_{\text{MF}} = -\frac{J_{\text{compr}}}{2N}\left[\sum_m^N s_1^{(m)}\right]^2 - \frac{J_{\text{shear}}}{2N}\sum_{\alpha=2}^{6}\left[\sum_m^N s_\alpha^{(m)}\right]^2 \tag{21}$$

where $\vec{s}^{(m)} \equiv \vec{g}^{(m)}/g$ are unit vectors and denominators $2N$ were introduced for convenience. Note that the coupling constants J

above are proportional to g^2, according to eq 18. The numerical value of the J_{compr}/J_{shear} ratio is equal to the ratio of the two distinct eigenvalues of the angular-averaged $\tilde{K}$ tensor:

$$\frac{J_{compr}}{J_{shear}} = \frac{5}{2}\frac{K}{K+2\mu} \equiv \frac{5}{2}\frac{1+\sigma}{4-5\sigma} \equiv \frac{5}{2}\frac{3-4c_t^2/c_l^2}{3+2c_t^2/c_l^2} \tag{22}$$

This ratio varies between 0.88 and 1.6 for nonmetallic glasses surveyed by Novikov and Sokolov.[36,37] Here, σ is the Poisson ratio, c_l and c_t are the longitudinal and transverse speeds of sound. Bigger values of the J_{compr}/J_{shear} ratio correspond to a greater Poisson ratio and smaller μ/K ratio, i.e., to a lower shear modulus relative to the bulk modulus. We thus observe that the mean-field Heisenberg model (21) has anisotropic couplings, the anisotropy directly related to the Poisson ratio of the material. Remarkably, the purely isotropic case $J_{compr}/J_{shear} = 1$ (corresponding to $\sigma = 1/5$, $c_t^2/c_l^2 = 3/8$) falls within the experimental range, the implications to be discussed at the end of the article.

The mean-field Hamiltonian (21) can be solved in a standard fashion by a Hubbard-Stratonovich transformation, so that the partition function is given the following six-dimensional integral, up to a multiplicative constant:

$$Z_{MF} = \sum_{\{\vec{s}^{(m)}\}} \int \prod_{\alpha=1}^{6} dh_\alpha \exp\left\{-N\frac{h_1^2}{2\beta J_{compr}} - N\sum_{\alpha=2}^{6}\frac{h_\alpha^2}{2\beta J_{shear}} + \sum_{\alpha=2}^{6} h_\alpha \sum_{m}^{N} s_\alpha^{(m)}\right\} \tag{23}$$

where the sum in front of the integral denotes averaging with respect to spin orientations. Equation 23 is a minor variation on the mean field solution of the isotropic Heisenberg model for an arbitrary number of vector-components, which can be found, for instance, in ref 28. Upon the angular averaging (see the derivation of eq 14), the integration can be done by steepest descent. In the leading order, the partition function is equal to $e^{-\beta N G_0}$, where G_0 is the minimum value of the following free energy:

$$\frac{G}{N} = \frac{h_c^2}{2\beta J_{compr}} + \frac{h_s^2}{2\beta J_{shear}} - \ln\frac{I_2(\sqrt{h_c^2+h_s^2})}{h_c^2+h_s^2} \tag{24}$$

with respect to the variables h_c and h_s (cf. eq 2.3 of ref 28). $h_c \equiv h_1$ gives the effective field on each spin in the direction of uniform compression/dilation; it can be of either sign. $h_s \equiv (\Sigma_{\alpha=2}^{6} h_\alpha^2)^{1/2}$ is the *magnitude* of the total field in the direction of pure shear and can be only non-negative, of course. The free energy from eq 24 is graphed in Figure 3 for two distinct values of anisotropy, at a temperature below the Curie temperature.

The Curie temperature itself, according to eq 24, is determined by the bigger of the two coupling constants:

$$k_B T_{Curie}^{MF} = \frac{1}{6}\max(J_{compr}, J_{shear}) \tag{25}$$

We remind the reader that the activated regime corresponds to the ordered state of the magnet. If $J_{compr} > J_{shear}$, the ordering is along the compression/dilation component of the local displacement, which corresponds to the first sum in eq 21; see Figure 3. Note the depths of the two minima are equal, implying there is no net volume change during the ordering transition. From the spin perspective, this state is essentially an ordered Ising ferromagnet. Conversely, if $J_{shear} > J_{compr}$, it is the shear component that becomes ordered; this component corresponds to the second sum in eq 21. The frozen-in shear state is an ordered 5-component Heisenberg ferromagnet, from the spin viewpoint. We summarize these notions graphically in the phase diagram shown in Figure 4.

We may further connect the mean-field parameters J_{shear} and J_{compr} to the material constants by enforcing the aforementioned notion that the large g asymptotic of the function $F_0(g)$ be logarithmic in the large g limit, i.e., when the vector length is

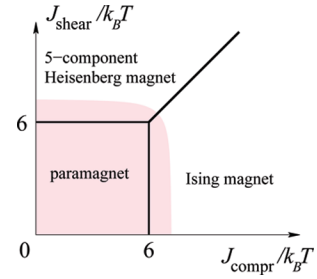

Figure 4. Phase diagram corresponding to the mean-field Hamiltonian (21). The shaded region schematically denotes the regime where the mapping between liquid dynamics and the spin model does not apply. Labels "Ising magnet" and "Heisenberg magnet" indicate ordering of the compression and shear components in eq 21 in the respective regions of the diagram.

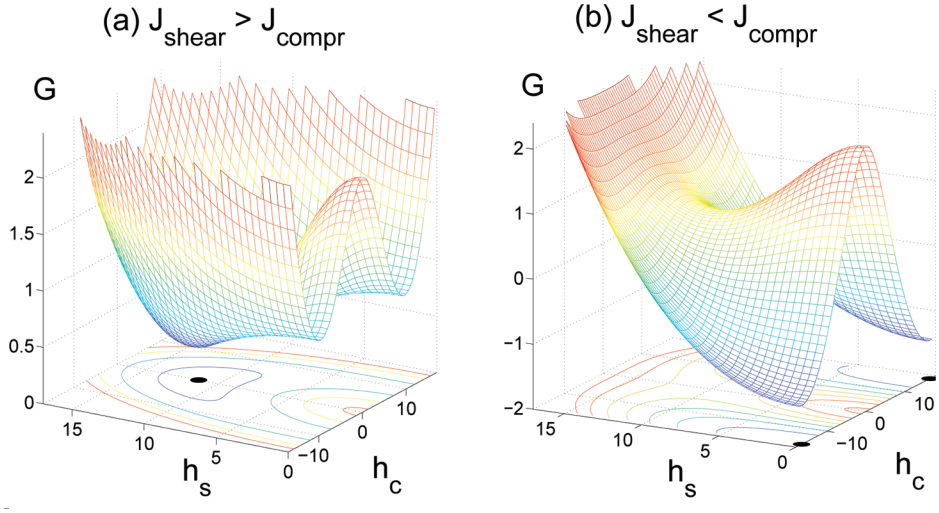

Figure 3. Free energy from eq 24 corresponding to the elastic constants of (a) silica ($J_{compr}/J_{shear} \simeq 0.88$) and (b) salol ($J_{compr}/J_{shear} = 1.5$), corresponding to a high and low values of the shear modulus, relative to the bulk modulus. (a) and (b) exhibit frozen-in shear and uniform compression/dilation, respectively. Solid circles at bottom plane denote the locations of minima.

large. According to eqs 14 and 24, the quadratic term in g from eqs 14 will cancel out at large g, if

$$\max(J_{\mathrm{compr}},J_{\mathrm{shear}}) = g^2a^3 \tag{26}$$

As a result,

$$g^2 = \frac{6k_{\mathrm{B}}T^{\mathrm{MF}}_{\mathrm{Curie}}}{a^3} \tag{27}$$

After comparing this equation with eq 17, we conclude that the mean-field Curie temperature of our magnet is significantly higher than the temperature at which the aperiodic stress pattern sets in, since the actual value of g in the metastable phase is significantly greater than the critical value from eq 17; see Figure 5. This notion confirms that, at least in the mean-field limit, our mapping activated transport onto an ordered spin model is internally consistent.

We further use the relation in eq 26 to compute the mean-field expression for $F_0(g)$ (by numerically minimizing the free energy from eq 24). The result is shown with the dash-dotted line in Figure 5. To compute the full free energy of the solid $F(g)$, from eq 3, we must make a specific assumption on the penalty $F_{\mathrm{ex}}(g)$ for dilating the sample. For the sake of argument, we have used a quadratic function $F_{\mathrm{ex}}(g)/Na^3 = cg^2$. A specific value $c = 0.05$ was chosen, so that the resulting barrier between the two phases is about $k_{\mathrm{B}}T$, since it is known that the one-particle barrier for surface melting is about $k_{\mathrm{B}}T$.[7]

The mean-field solution supports the asymptotic analysis from section 2 that the fully mechanically stable solid is indeed the lowest free energy state; whereas the aperiodic state, though significantly higher in free energy, is metastable owing to the surface tension between the two phases.

4. Summary and Discussion

We have mapped the liquid activated-transport regime onto the dynamics of a spin model on a *fixed* lattice. The long-lived aperiodic arrangements, which are characteristic of the activated regime, correspond to aperiodic spin configurations below the Curie point of the spin system. The presence of nonzero shear resistance in the long-lived structures is reflected in the spins having six components, which correspond to the six independent entries of the local deformation tensor. Each spin corresponds to a rigid, weakly interacting molecular units (or "bead") of the ROFT theory. The size of the bead is set unambiguously as the length scale of the inhomogeneity of a frozen-in stress distribution in the activated regime. The length of the vectors is determined self-consistently as the value of the order parameter for the periodic-to-aperiodic crystal transition. The mutual angles between spins change little during the cooperative reconfigurations, implying individual bonds are deformed nearly harmonically most of the time. The anharmonicity of the reconfigurations is reflected in a high nucleation barrier in the free energy profile of the transition, the progress coordinate being the number of beads that have already switched their positions to their value in the new arrangement. The present approach exhibits clear parallels with earlier, self-consistent phonon theories of aperiodic crystals,[1,19] which considered the uniform liquid state as the reference state and have demonstrated that the uniform liquid can crossover to an aperiodic-crystal state, accompanied by a discontinuous change of an order parameter corresponding to the bead localization length. In contrast, here we construct the aperiodic crystal using a fully mechanically stable state as the starting point, thus allowing for a straightforward treatment of local, high-frequency shear resistance. We have also explicitly demonstrated that aperiodic crystals exhibit multiply degenerate states whose mutual interconversions can be mapped onto the dynamics of long-range, 6-spin model with anisotropic interactions.

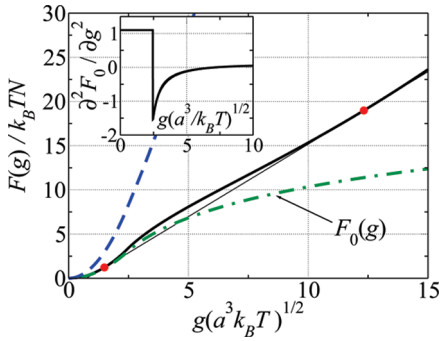

Figure 5. The dashed-dotted line shows the mean-field expression for the $F_0(g)$ function. The thick solid line shows the full free energy from eq 3, with a specific choice of the function $F_{\mathrm{ex}}(g)/N = c(g^2a^3)$, where the coefficient $c = 0.05$. The thin solid line is the common tangent of the two portions on the $F(g)$ that correspond to the mechanically stable reference state and the aperiodic metastable state. The dashed line shows the curve with the largest value of this coefficient ($c = 5/3$), at which the $F(g)$ curve still exhibits a nonconcave portion. In the inset, we plot the second derivative of the mean-field $F_0(g)$. The discontinuity is at $g^2a^3/k_{\mathrm{B}}T = 6$, cf. eq 27).

The present microscopic picture has implications for the temperature dependence of the activated barriers in supercooled melts that we can begin to discuss already at the mean-field level. In the allowed part of the phase diagram in Figure 4, consider a transition from the $J_{\mathrm{compr}} < J_{\mathrm{shear}}$ sector to the $J_{\mathrm{compr}} > J_{\mathrm{shear}}$ sector. As already mentioned, this transition would correspond to ordering of an Ising-like assembly of spins and vice versa for the 5-component Heisenberg spins. To avoid confusion, we emphasize that this Ising-like ordering takes place along one component of randomly oriented, *six*-component vectors. Now, according to accurate calculations,[38] the heat capacity jump upon ordering in the classical Heisenberg model tends to increase with lowering the dimensionality of the spins and reaches its largest value in the Ising model. This implies that the rhs part of the phase diagram should generically exhibit a higher specific heat. In view of the RFOT-derived connection between the fragility index and the heat capacity jump, i.e., the mentioned $m \simeq 34.7\Delta c_p$ relation, we may expect that substances with a larger $J_{\mathrm{compr}}/J_{\mathrm{shear}}$ ratio will generically be more fragile, but under several, rather restrictive circumstances, as we discuss next.

First, we reiterate the present approach is a minimalist way to explicitly account for the interactions that give rise to (high frequency) shear resistance in supercooled liquids. Already in this minimal model, the entropy and heat capacity per bead depend on the bead size a, which is, formally, the ultraviolet cutoff in the theory. In addition to the purely volumetric affect (one vector occupies a volume a^3) the bead size will affect the precise, self-consistently determined value of the order parameter g in the glass phase. Further, the isotropic assumption for local elastic response, from eq 11, is an approximation. Contributions other than purely elastic terms in eq 6 will be generally present as well. One source of such contribution is the reconfiguration-induced electric dipole moment. Earlier estimates[39] suggest that even though the local polarization resulting from bead movements contributes only about a percent to local elastic constants, the resulting elemental electric dipoles interact comparably strongly to the elastic dipoles of the type we have considered. This effect should be especially significant in ionic glasses.[16]

Interestingly, because of the mentioned antiferromagnetism of the electric dipoles, the electric and elastic interactions may be mutually frustrating. A careful treatment of polymeric materials, on the other hand, should include the effects of chain rigidity and other types of local anisotropy that could not be accounted for by only two elastic constants and the bead size a, which are the parameters of our ansatz. Novikov and Sokolov have argued electronic contributions must be considered in metallic glasses.[40]

According to Figure 4, we should expect that actual substances will exhibit a continuous range of local stress distributions and heat capacities. Indeed, to distinct points on the phase diagram in Figure 4, there correspond very different values of the heat capacity. Furthermore, the heat capacity of an anisotropic Heisenberg model on a periodic lattice should exhibit a nonmonotonic behavior as a function of anisotropy, namely a spike at a transition that would occur at $J_{\mathrm{compr}} = J_{\mathrm{shear}}$ in the mean-field limit. $J_{\mathrm{compr}} = J_{\mathrm{shear}}$ corresponds to the following value of the ratio of the longitudinal and transverse velocities: $c_l/c_t \simeq 1.63$. This is roughly consistent with a very broad range of fragilities observed for substances from a relatively narrow range of the c_l/c_t ratio centered at 1.75 or so.[41] We point out that the correlation between the Poisson ratio and the fragility has been a subject of debate for some time.[36,37,40−43] Our results suggest that a correlation between the fragility and the Poisson ratio might in fact be expected for nonmetallic substances that are far from the transition region $J_{\mathrm{compr}} = J_{\mathrm{shear}}$. Yet for substances near the "critical region" $J_{\mathrm{compr}} = J_{\mathrm{shear}}$, little correlation is expected. Note that the view of the activated regime in a *fragile* substance as a random Ising model below symmetry breaking is consistent with recent results of Stevenson et al.[44] who have mapped the localization transition in fiducial liquid structures of a Lennard-Jones mixture onto a replica-symmetry breaking transition in a random Ising model.

Regardless of the detailed value of the heat capacity, our results indicate that supercooled liquids exhibit local stress distribution ranging from frozen-in compression to frozen-in shear. Furthermore, the present findings that the activated liquid regime arises self-consistently from a mechanically stable reference state merge nicely with the self-consistent phonon view of the emergence of the aperiodic crystal state from the uniform *liquid*.[1,19] This notion suggests that a unified, quantitative treatment of the liquid, aperiodic-crystal, and periodic-crystal regimes is in sight. We conclude by reiterating that despite system-specific variations in direct interactions, accounted for, semiempirically, in the variation of the elastic constants in Figure 4, the underlying mechanism of activated transport in nonpolymeric liquids is system-independent, consistent with the conclusions of the RFOT theory.

Acknowledgment. We gratefully acknowledge the Arnold and Mabel Beckman Foundation Beckman Young Investigator Award, the Donors of the American Chemical Society Petroleum Research Fund, and the Small Grant and GEAR Programs at the University of Houston, for partial support of this research.

Appendix A. Voigt−Mandel Notation

It is sometimes convenient to present the six independent entries of a symmetric tensor u_{ij} as a six-component vector:

$$\{u_{ij}|i,j=1,2,3\} \rightarrow \vec{t} \equiv \begin{pmatrix} u_{11} \\ u_{22} \\ u_{33} \\ \sqrt{2}u_{23} \\ \sqrt{2}u_{31} \\ \sqrt{2}u_{12} \end{pmatrix} \tag{28}$$

so that the convolution $u_{ij}\Lambda_{ijkl}u_{kl}$ is expressed as bilinear form $\sum_{\alpha,\beta=1}^{6} t_\alpha \Lambda_{\alpha\beta} t_\beta$, where $\Lambda_{\alpha\beta}$ is a square 6×6 matrix:

$$\begin{pmatrix} \Lambda_{1111} & \Lambda_{1122} & \Lambda_{1133} & \sqrt{2}\Lambda_{1123} & \sqrt{2}\Lambda_{1131} & \sqrt{2}\Lambda_{1112} \\ \Lambda_{2211} & \Lambda_{2222} & \Lambda_{2233} & \sqrt{2}\Lambda_{2223} & \sqrt{2}\Lambda_{2231} & \sqrt{2}\Lambda_{2212} \\ \Lambda_{3333} & \Lambda_{3322} & \Lambda_{3333} & \sqrt{2}\Lambda_{3323} & \sqrt{2}\Lambda_{3331} & \sqrt{2}\Lambda_{3312} \\ \sqrt{2}\Lambda_{2311} & \sqrt{2}\Lambda_{2322} & \sqrt{2}\Lambda_{2333} & 2\Lambda_{2323} & 2\Lambda_{2331} & 2\Lambda_{2312} \\ \sqrt{2}\Lambda_{3111} & \sqrt{2}\Lambda_{3122} & \sqrt{2}\Lambda_{3133} & 2\Lambda_{3123} & 2\Lambda_{3131} & 2\Lambda_{3112} \\ \sqrt{2}\Lambda_{1211} & \sqrt{2}\Lambda_{1222} & \sqrt{2}\Lambda_{1233} & 2\Lambda_{1223} & 2\Lambda_{1231} & 2\Lambda_{1212} \end{pmatrix} \tag{29}$$

In the isotropic case, eq 11, this matrix is rather sparse and easily shown to have one eigenvalue 3K and a 5-fold degenerate eigenvalue 2μ. Importantly, the corresponding orthogonal transformation matrix, i.e., the matrix consisting of the eigenvectors of the matrix from eq 29 for an isotropic Λ, *does not depend on the K/μ ratio*. (The transformation matrix is easy to compute but is too bulky to give here.) This means, among other things, that in the Voigt basis, *all* isotropic interactions are diagonal.

One may further rescale the components of the 6-vectors, for a specific combination of K and μ:

$$\vec{g} = \begin{pmatrix} \sqrt{K}(d_{11} + d_{22} + d_{33}) \\ \sqrt{\mu}(d_{11} - d_{22}) \\ \sqrt{\frac{\mu}{3}}(d_{11} + d_{22} - 2d_{33}) \\ 2\sqrt{\mu}d_{23} \\ 2\sqrt{\mu}d_{31} \\ 2\sqrt{\mu}d_{12} \end{pmatrix} \tag{30}$$

so as to make the matrix from eq 29 not only diagonal but also unit: $d_{ij}\Lambda_{ijkl}\, d_{kl} = \vec{g}^2 \equiv \sum_{\alpha=1}^{6} g_\alpha{}^2 \equiv g^2$ (and similarly for the elastic components); see eqs 9 and 10.

Appendix B. Spin−Spin Interaction

To evaluate the coupling between the nonlinear oscillators, we integrate out only the phonon degrees of freedom $\mathbf{u}$ in eq 4; i.e., we need to perform the following functional integral:

$$\int [\Pi_{\mathrm{r}}\, \mathrm{d}^3\mathbf{u}(\mathbf{r})] \exp\{-\beta[\int \mathrm{d}^3\mathbf{r}\, (u_{ij}\Lambda_{ijkl}u_{kl}/2) + \sum_m a^3\, d_{ij}(\mathbf{r}_m)\, \Lambda_{ijkl} u_{kl}(\mathbf{r}_m)]\} \tag{31}$$

where the m-summation is over the locations $\boldsymbol{r}_{\mathrm{m}}$ of the harmonic oscillators. (Note the $\mathrm{d}\Lambda u$ cross-term is symmetrized because $\Lambda_{ijkl} = \Lambda_{klij}$.) In terms of the Fourier components of the local displacements $\mathbf{u}$: $\tilde{\mathbf{u}}(\mathbf{k}) = \int \mathrm{d}^3\mathbf{r}\, \mathbf{u}(\mathbf{r}) \mathrm{e}^{\mathrm{i}\mathbf{k}\mathbf{r}}$, this integral becomes

$$\int [\Pi_k \, \mathrm{d}^3\tilde{u}(\boldsymbol{k})] \exp\left\{-\beta \int \frac{\mathrm{d}^3\mathbf{k}}{(2\pi)^3}[\Lambda_{njlm}\tilde{u}_n(\mathbf{k})\, \tilde{u}_l(-\mathbf{k})k_j k_m/2 + \sum_m a^3 d_{nj}(\mathbf{r}_m)\, \Lambda_{njlp}(-\mathrm{i}k_l)\tilde{u}_p \mathrm{e}^{-\mathrm{i}\mathbf{k}\mathbf{r}_m}]\right\} \quad (32)$$

where an appropriate ultraviolet cutoff at k_{micro}, as in eq 19, is understood. (Note $\Lambda_{ijkl} = \Lambda_{jikl}$, $\Lambda_{ijkl} = \Lambda_{ijlk}$.) For the specific, simple form of the elastic tensor Λ from eq 11, it is straightforward to compute the Gaussian integral above explicitly, using the obvious property of the Fourier component of the real-valued displacements $\mathbf{u}$: $\tilde{\mathbf{u}}(-\mathbf{k}) = \tilde{\mathbf{u}}^*(\mathbf{k})$, and Hubbard−Stratonovich formulas $\int_{-\infty}^{\infty}(\mathrm{d}x\mathrm{d}y/\pi) \exp[-(x^2 + y^2) + a(x - \mathrm{i}y) + b^*(x + \mathrm{i}y)] = \mathrm{e}^{ab^*}$ and $\int_{-\infty}^{\infty}(\Pi_m \, \mathrm{d}x_m/\pi^{1/2})\mathrm{e}^{-x_k A_{kl} x_l + b_k x_k} = (\mathrm{Det}\, A)^{-1/2}\mathrm{e}^{b_k A_{kl}^{-1} b_l/4}$, where $\{A_{kl}\}$ is a positively defined symmetric matrix. The inverse of the matrix $A_{il} \equiv \Lambda_{ijlm}k_j k_m$ is easy to find, using the special property of the matrix $P_{jm} \equiv k_j k_m/k^2 \equiv \hat{k}_j\hat{k}_m$ that $P^2 = P$. Using this notion, one may show that

$$(\Lambda_{ijlm}\hat{k}_j\hat{k}_m)\left(\delta_{\mathrm{ln}} - \frac{\lambda + \mu}{\lambda + 2\mu}\hat{k}_l\hat{k}_n\right) = \delta_{in} \quad (33)$$

where Λ_{ijkl} is from eq 11. Finally note that the k-integration in the exponent in eq 32 counts every phononic mode twice, because of the mentioned property $\tilde{\mathbf{u}}(-\mathbf{k}) = \tilde{\mathbf{u}}^*(\mathbf{k})$. ($\mathrm{d}^3\tilde{\mathbf{u}}(\mathbf{k}) \equiv \{\mathrm{d}^3 \mathrm{Re}\,[\tilde{\mathbf{u}}(\mathbf{k})]\mathrm{d}^3 \mathrm{Im}\,[\tilde{\mathbf{u}}(\mathbf{k})]\}^{1/2}$.) We use the listed notions to perform the functional integration in eq 32 and thus arrive at eq 18 of the main text.

It may be instructive to compare the straightforward, if not somewhat tedious calculation above with a simpler case of interaction between 3-component vectors mediated by a single-polarization elastic interaction:

$$E = \int \mathrm{d}V\, [K(\nabla\psi)^2/2 + \sum_m (\mathbf{g}^{(m)}\nabla\psi)\delta^3(\mathbf{r} - \mathbf{r}_m)] \quad (34)$$

where $\psi \equiv \psi(\mathbf{r})$ is a coordinate dependent, scalar field. In this case, the phonon-mediated coupling between the spins becomes

$$\mathscr{H} = -\sum_{m<n} a^3 J_{ij}(\mathbf{r}_{mn}) g_i^{(m)} g_j^{(n)} \quad (35)$$

This coupling looks particularly simple in the Fourier domain: $J_{ij}(\mathbf{r}_{mn}) = \int \mathrm{d}^3(ka)/(2\pi)^3 \cos(\mathbf{kr})\hat{k}_i\hat{k}_j$; at distances well-exceeding the inverse ultraviolet cutoff, it is identical to the usual electric dipole−dipole interaction, albeit with the opposite sign: $J_{ij}(\mathbf{r}_{mn}) \equiv (\delta_{ij} - 3n_i n_j)/{r_{mn}}^3$, where $\mathbf{r}_{mn} \equiv (\mathbf{r}_m - \mathbf{r}_n)$ and $n \equiv \mathbf{r}_{mn}/r_{mn}$. It is easy to show, by a direct calculation, that the eigenvalues of the matrix $\hat{k}_i\hat{k}_j$ are 1, 0, 0.

To perform the angular averaging of the tensor $\tilde{K}$ in eq 19, one needs to compute $\langle\hat{k}_i\hat{k}_j\rangle$ and $\langle\hat{k}_i\hat{k}_j\hat{k}_l\hat{k}_m\rangle$, where the angular brackets $\langle\cdots\rangle$ denote angular averaging. To compute these averages, we note that by symmetry $\langle\hat{k}_i\hat{k}_j\rangle \propto \delta_{ij}$, and that $\hat{k}_i{}^2 = 1$, implying $\langle\hat{k}_i\hat{k}_j\rangle = (1/3)\delta_{ij}$. By the same token, since $\langle\hat{k}_i\hat{k}_j\hat{k}_l\hat{k}_m\rangle \propto (\delta_{ij}\delta_{lm} + \delta_{im}\delta_{jl})$ and $\hat{k}_i{}^2\hat{k}_j{}^2 = 1$, we obtain $\langle\hat{k}_i\hat{k}_j\hat{k}_l\hat{k}_m\rangle = (1/15)\,(\delta_{ij}\delta_{lm} + \delta_{il}\delta_{jm} + \delta_{im}\delta_{jl})$. Using these expressions and eq 11, we obtain $\langle\tilde{K}_{ijkl}\rangle = \lambda'\delta_{ij}\delta_{kl} + \mu'(\delta_{ik}\delta_{jl} + \delta_{il}\,\delta_{jk})$, where $\lambda' = (\lambda^2 + 16\lambda\mu/15 - 4\mu^2/15)/(\lambda + 2\mu)$ and $\mu' = 2\mu\,(3\lambda + 8\lambda)/15(\lambda + 2\mu)$. Therefore the $\langle\tilde{K}_{ijkl}\rangle$ tensor has the same structure as the tensor itself and will be diagonal in the Voigt representation, after a basis change as in eq 30. Of the corresponding diagonal entries, one is $K/(\lambda + 2\mu)$ and the rest five are $(2/5)(K + 2\mu)/(\lambda + 2\mu)$, as mentioned in the main text. We note that the sum of the diagonal entries is equal to 3, as expected from the discussion in the beginning of section 3.

References and Notes

(1) Singh, Y.; Stoessel, J. P.; Wolynes, P. G. *Phys. Rev. Lett.* **1985**, *54*, 1059–1062.
(2) Lubchenko, V.; Wolynes, P. G. *J. Chem. Phys.* **2003**, *119*, 9088–9105.
(3) Casalini, R.; Paluch, M.; Roland, C. M. *J. Chem. Phys.* **2003**, *118*, 5701.
(4) Kirkpatrick, T. R.; Wolynes, P. G. *Phys. Rev. A* **1987**, *35*, 3072–3080.
(5) Kirkpatrick, T. R.; Wolynes, P. G. *Phys. Rev. B* **1987**, *36*, 8552–8564.
(6) Lindemann, F. A. *Phys. Z.* **1910**, *11*, 609.
(7) Lubchenko, V. *J. Phys. Chem. B* **2006**, *110*, 18779–18786.
(8) Kirkpatrick, T. R.; Thirumalai, D.; Wolynes, P. G. *Phys. Rev. A* **1989**, *40*, 1045–1054.
(9) Xia, X.; Wolynes, P. G. *Proc. Natl. Acad. Sci. U.S.A.* **2000**, *97*, 2990–2994.
(10) Lubchenko, V.; Wolynes, P. G. *J. Chem. Phys.* **2004**, *121*, 2852.
(11) Lubchenko, V.; Wolynes, P. G. *Annu. Rev. Phys. Chem.* **2006**, *58*, 235–266.
(12) Martinez, L.-M.; Angell, C. A. *Nature* **2001**, *410*, 663.
(13) Angell, C. A. *J. Non-Cryst. Solids.* **1985**, *73*, 1–17.
(14) Stevenson, J.; Wolynes, P. G. *J. Phys. Chem. B* **2005**, *109*, 150.
(15) Hall, R. W.; Wolynes, P. G. *Phys. Rev. Lett.* **2003**, *90*, 085505.
(16) Lubchenko, V. *J. Chem. Phys.* **2007**, *126*, 174503.
(17) Turnbull, D. *J. Appl. Phys.* **1950**, *21*, 1022.
(18) Zhugayevych, A.; Lubchenko, V. Submitted to *J. Chem. Phys.*
(19) Hall, R.; Wolynes, P. *J. Chem. Phys.* **1987**, *86*, 2943–2948.
(20) Rowlinson, J. S.; Widom, B. *Molecular Theory of Capillarity*; Clarendon Press: Oxford, U.K., 1982.
(21) Loidl, A. *Annu. Rev. Phys. Chem.* **1989**, *40*, 29–60.
(22) Cochran, W. *Phys. Rev. Lett.* **1959**, *3*, 412–414.
(23) Bales, G. S.; Gooding, R. J. *Phys. Rev. Lett.* **1991**, *67*, 3412–3415.
(24) Lookman, T.; Shenoy, S. R.; Rasmussen, K. O.; Saxena, A.; Bishop, A. R. *Phys. Rev. B* **2003**, *67*, 024114.
(25) Landau, L. D.; Lifshitz, E. M. *Theory of Elasticity*; Pergamon Press: Oxford, U.K., 1986.
(26) Mehrabadi, M. M.; Cowin, S. C. *J. Mech. Appl. Math.* **1990**, *43*, 15.
(27) Mandel, J. *J. Mècanique* **1962**, *1*, 3.
(28) Nobre, F. D.; Tsallis, C. *Phys. Rev. E* **2003**, *68*, 036115.
(29) Abramowitz, A., Stegun, I., Eds. *Handbook of Mathematical Functions*; Dover: Boston, 1964.
(30) Schmalian, J.; Wolynes, P. G. *Phys. Rev. Lett.* **2001**, *85*, 3456.
(31) Monasson, R. *Phys. Rev. Lett.* **1995**, *75*, 2847–2850.
(32) Grannan, E. R.; Randeria, M.; Sethna, J. P. *Phys. Rev. B* **1990**, *41*, 7784–7798.
(33) Grannan, E. R. Low Temperature Properties of Glasses. Ph.D. thesis, Cornell University, 1989.
(34) Yu, C. C. *Phys. Rev. Lett.* **1992**, *69*, 2787–2790.
(35) Luttinger, J. M.; Tisza, L. *Phys. Rev.* **1946**, *70*, 954–964.
(36) Novikov, V. N.; Sokolov, A. P. *Nature* **2004**, *431*, 961.
(37) Sokolov, A. P.; Novikov, V. N.; Kisliuk, A. *Philos. Mag.* **2007**, *87*, 613–621.
(38) Usatenko, Z. E.; Kozlovskii, M. P. *Phys. Rev. B* **2000**, *62*, 9599–9615.
(39) Lubchenko, V.; Silbey, R. J.; Wolynes, P. G. *Mol. Phys.* **2006**, *104*, 1325.
(40) Novikov, V. N.; Sokolov, A. P. *Phys. Rev. B* **2006**, *74*, 064203.
(41) Johari, G. P. *Philos. Mag.* **2006**, *86*, 1567–1579.
(42) Torchinsky, D. H.; Johnson, J. A.; Nelson, K. A. *J. Chem. Phys.* **2009**, *130*, 064502.
(43) Yannopoulos, N.; Johari, G. P. *Nature* **2006**, *442*, E7–E8.
(44) Stevenson, J. D.; Walczak, A. M.; Hall, R. W.; Wolynes, P. G. *J. Chem. Phys.* **2008**, *129*, 194505.

JP9070345